AAS 21-712

MODELLING THE WHOLE SPACE DEBRIS ENVIRONMENT THROUGH A SPATIAL DENSITY APPROACH

Cristina Duran[*], Lorenzo Giudici[†], Camilla Colombo[‡]

This paper proposes a continuum density approach for analyzing the impact of a fragmentation event into the global debris environment. The debris population in LEO is represented through its spatial density, defined as a function depending only on the radial distance from the Earth. The time evolution of the density function is modelled through the continuity equation, considering the atmospheric drag effect. At a certain instant, a fragmentation cloud is generated. After the band formation, its contribution is added to the background population, analyzing the evolution of the total spatial density function. Finally, a novel formulation is introduced to also take into account the effect of the secondary phenomena derived from a collision or explosion in space. In particular, a chain of concatenated collisions, triggered by a single original fragmentation event, is considered, as well as its feedback effect on the overall debris population. Results are presented for three different scenarios to illustrate the long-term repercussions of fragmentation events.

INTRODUCTION

Since the first satellite was launched in 1957, the number of man-made objects in Earth orbit has been exponentially increasing.[1] Nowadays, space debris constitutes a real threat for space activities and space agencies are cooperating to identify appropriate space debris mitigation measures. Within this context, explosions of the abandoned spacecraft or upper rocket stages composing the debris population, as well as collisions between them and other objects orbiting around the Earth, might have a fatal impact into the space environment, generating hundreds of thousands of fragments with a diameter larger than 1 mm.[2]

Several methods have been developed in order to estimate the long-term consequences of such fragmentation clouds. Evolutionary debris models generally rely on semi-analytical methods to propagate the dynamics of space debris under orbit perturbations.[3–5] To ensure the robustness of the results against uncertainties and to overcome the absence of a complete set of experimental data, these methods use several Monte Carlo runs in order to consider a large number of possible evolution scenarios of the debris population.[3,6,7] This considerably increases the required computational time and, thus, limits the variety of possible analyses. In this paper, a continuum approach is employed to predict the evolution of debris clouds in Low Earth Orbit (LEO). Instead of separately propagating the trajectory of an extensive set of objects, here the cloud behavior is studied globally, which allows massive sets of debris data to be handled within a reasonable computational time.

[*]MSc student, Dept. of Aerospace Science & Technology, Politecnico di Milano, Via La Masa 34, 20156 Milano, Italy.
[†]PhD researcher, Dept. of Aerospace Science & Technology, Politecnico di Milano, Via La Masa 34, 20156 Milano, Italy.
[‡]Associate professor, Dept. of Aerospace Science & Technology, Politecnico di Milano, Via La Masa 34, 20156 Milano, Italy.

In this paper, the approach in Letizia et al.[8] for continuum modelling of fragmentation clouds is modified and extended to the study of the global debris population. A density-based approach is employed in order to analyze the effect of a fragmentation event on the overall debris population (the IADC population is considered), taking as starting point the strategy in Colombo et al.[9]

The debris population in LEO is represented through its spatial density, defined as a function depending only on the radial distance from the Earth. The time evolution of this function is modelled, under the assumption of quasi-circular orbits, through the continuity equation, considering the effect of atmospheric drag.[10] Simultaneously, the NASA breakup model[2] is used to characterize the fragments generated from a certain collision or explosion. The orbital elements of the produced fragments are propagated, considering atmospheric drag and J_2 perturbations, up to the band formation, when the continuum formulation in McInnes[10] becomes applicable also for the fragmentation cloud. At this time instant, the spatial density function of the fragmentation is built and its contribution is added to the background debris population. The resulting spatial density function is propagated again, obtaining the evolution in time of the total debris population.[10] Finally, a novel formulation, based on the approach in Somma et al.,[11] is introduced to also take into account the effect of the secondary phenomena derived from a collision or explosion in space. In particular, a chain of concatenated collisions, triggered by a single original fragmentation event, is considered, as well as its feedback effect on the overall population in LEO.

CONTINUUM FORMULATION FOR A FRAGMENTATION EVENT

Taking as starting point the strategy proposed in Letizia et al.,[8] an efficient method is developed, to describe the time evolution of the fragmentation cloud resulting from a collision or explosion in space. The algorithm implementing this method is structured according to the following blocks (see Figure 1):

- A breakup model, that characterizes the generated fragments, given the initial conditions under which the fragmentation event takes place.
- A numerical long-term propagator to determine the evolution in time of the orbital elements of the produced fragments, until the continuum formulation in McInnes[10] becomes applicable.
- The spatial density function, defined to translate the orbital parameters of each single fragment into a continuous function depending only on the radial distance from the Earth.
- A numerical continuum propagator to describe the evolution in time of the spatial density function, from the band formation instant onward.

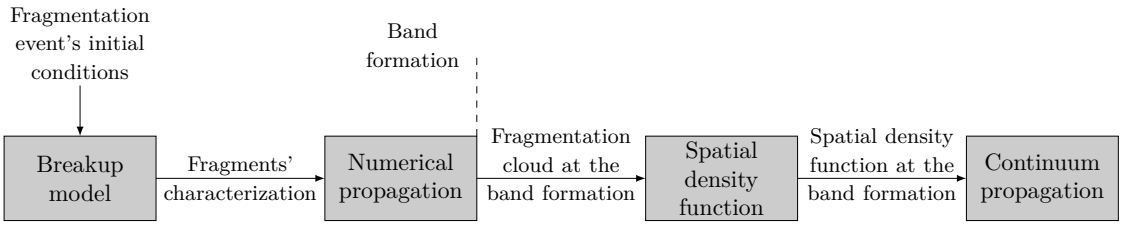

Figure 1: Schematics of the algorithm for the propagation of the fragmentation cloud.

NASA Breakup model

The fragmentation event, collision or explosion, is here modelled through the standard NASA breakup model.[2,12] According to the implementation in Krisko,[12] the number of produced fragments, N_f, of a given characteristic length L_c or larger can be computed through Equation 1, depending on the nature of the considered fragmentation event:

$$\begin{aligned} \text{Explosion}: \quad & N_f = 6S(L_c[\text{m}])^{-1.6} \\ \text{Collision}: \quad & N_f = 0.1(M_e[\text{kg}])^{0.75}(L_c[\text{m}])^{-1.71} \end{aligned} \tag{1}$$

with S an empirically derived unitless factor between 0.1 and 1 (dependent on the explosive body type) and the reference mass of the collision, M_e, defined according to the expressions in Equation 2. Here, a catastrophic collision is considered for values of the impact energy per target mass exceeding 40 J/g, since, under these conditions, the collision is assumed to cause the complete fragmentation of both the impactor and the target.[6]

$$\begin{aligned} \text{Catastrophic collision}: \quad & M_e[\text{kg}] = M_t[\text{kg}] + M_p[\text{kg}] \\ \text{Non}-\text{catastrophic collision}: \quad & M_e[\text{kg}] = M_p[\text{kg}](v_c[\text{km/s}]/1[\text{km/s}])^2 \end{aligned} \tag{2}$$

where M_t is the target mass, M_p is the projectile mass and v_c is the relative impact velocity between the projectile and the target.

The area-to-mass ratio A/M distribution is modelled as a lognormal distribution function, with mean value $\mu_{A/M}$ [m^2/kg] and standard deviation $\sigma_{A/M}$ [m^2/kg]. Expressions for these parameters can be found in Johnson and Krisko,[2] for the three different types of considered objects (rocket bodies, spacecraft and small objects).

The magnitude of the velocity variation caused by the fragmentation, Δv, is defined as a function of the area-to-mass ratio and, similarly, its distribution is modelled as a lognormal distribution function. Again, the expressions for the mean value $\mu_{\Delta v}$ [km/s] and the stardard deviation $\sigma_{\Delta v}$ [km/s] characterizing this distribution are taken from Johnson and Krisko.[2]

Following the strategy in Letizia,[13] in this work, the Δv direction is randomized and a limitation to the maximum velocity variation is imposed (equal to $1.3v_c$) since, otherwise, the method would generate a small set of fragments with very high ejection velocity (in the order of 60 km/s). Despite the weaknesses of the NASA breakup model,[13] it does not represent a limitation for the approach here presented. The continuum method proposed in this work does not rely on a specific breakup model: any alternative model could be implemented by replacing only the first block in Figure 1, whereas the other blocks would remain unchanged (see Olivieri et al.[14]).

Band formation and numerical propagation

Phases of the evolution of a debris cloud in LEO

The dispersion model of a fragmentation cloud in LEO can be divided into four phases.[15] In the first phase, right after the fragmentation event, the produced fragments form an ellipsoid-shaped cloud, concentrated at the location where the collision or explosion took place. The energy differences among the generated fragments and, hence, their variable orbital periods, cause the initial cloud to be spread out along the parent orbit, forming a toroid (phase two). During phase three, the toroid is gradually dismantled, due to the change of the right ascension of the ascending node, Ω, and the variation of the argument of perigee, ω, both caused by the Earth's oblateness. In the

final configuration (phase four), the cloud forms a band around the Earth, limited in latitude by the inclination of the parent orbit. Throughout this phase, atmospheric drag can be assumed to be the dominant perturbation,[15] since ω, Ω and the true anomaly, θ, are randomized.

Consequently, the continuum formulation in McInnes,[10] which takes into account only the atmospheric drag effect, can be applied only after the band formation, while a numerical propagator is needed to follow the first phases of the cloud evolution.

Adopting the approach in Letizia et al.,[8] the band formation time is estimated as $T_B = 3T_b$, where T_b is the expression for the band formation time proposed by Ashenberg.[16]

Numerical propagation

Once the fragments are generated and characterized, their associated position and velocity vectors are computed; the fragments are assumed to suffer an instantaneous velocity variation without position change. Then, the Keplerian elements defining each fragment's orbit right after the fragmentation event are obtained.

The evolution in time of the fragment's orbital elements is computed through the numerical integration of the Gauss' planetary equations,[17] considering atmospheric drag and Earth's oblateness perturbations. Drag effect is estimated assuming an exponential density model:[17]

$$\rho = \rho_{ref} \exp\left(-\frac{h - h_{ref}}{H}\right) \tag{3}$$

where ρ is the atmospheric density, h is the altitude and h_{ref} is the reference altitude where the reference density ρ_{ref} and the scale height H are defined. The reference values are taken from Vallado.[17] Following the approach in Letizia et al.,[8] in this work, the reference altitude h_{ref} is selected as the closest tabulated value to the altitude where the fragmentation event takes place and its value is kept constant for the entire simulation; drag effect is considered up to a 1000 km altitude and atmosphere rotation is not taken into account.

The effect of atmospheric drag is computed through the expressions reported in King-Hele,[18] describing the secular variation of the orbital elements. Regarding the Earth's oblateness perturbation, only the secular effect of J_2 is considered. This assumption is made since, over the long-term, the Earth's oblateness only affects ω and Ω and, consequently, high-precision modelling of this perturbation is not essential.

The set of resulting differential equations is numerically integrated up to the band formation time. The numerical integration process is halted if the fragment's perigee altitude falls below 50 km, since, under this condition, the fragment is considered to be re-entering through the atmosphere.[8]

Spatial density function

Once the band is formed, the information on each single fragment is translated into a total continuous density function. Here, the spatial density function is built on the probability of finding a fragment at a distance r from the center of the Earth, given the semimajor axis a and the eccentricity e of its orbit. Taking the expression reported in Kessler,[19] the spatial density function $n_i(r)$ defining the contribution of fragment i is

$$n_i(r) = \frac{1}{4\pi^2 r a_i \sqrt{(r - r_{p_i})(r_{a_i} - r)}} \tag{4}$$

where r_{p_i} and r_{a_i} are, respectively, the periapsis and the apoapsis of the fragment's orbit:

$$\begin{aligned} r_{p_i} &= a_i(1 - e_i) \\ r_{a_i} &= a_i(1 + e_i) \end{aligned} \tag{5}$$

In order to build the total spatial density function, used as initial condition for the continuum propagation, the contribution of each fragment in the fragmentation cloud must be considered:

$$n(r) = \sum_{i=1}^{N} n_i(r) \tag{6}$$

where N is the total number of objects constituting the fragmentation cloud at the band formation.

Continuum propagation

Once the spatial density function is built at the band formation instant, the continuity equation is used to compute the density function evolution in time, under the effect of atmospheric drag. Here, the approach developed by McInnes[10] is followed. However, instead of using the analytical expression therein for the density function propagation, the derived differential equations are numerically integrated, from the band formation instant onward, as previously done in Frey et al.[20] Despite the consequent increase on the computational time, the numerical approach constitutes a step forward in terms of versatility, allowing for the propagation of the continuity equation with source-sink terms, as well as a wider variety of orbit perturbations (considering more sophisticated force models) and orbit geometries.

The continuity equation (traditionally used in fluid dynamics) provides a description of the evolution of the density of a continuum, given the velocity of its constituting particles. In particular, if n represents a generic density function, the continuity equation can be written as[10]

$$\frac{\partial n}{\partial t} + \nabla \cdot (n\mathbf{f}) = \dot{n}^{+} - \dot{n}^{-} \tag{7}$$

where t is the time, the term $\nabla \cdot (n\mathbf{f})$ models the forces acting on the system and accounts for *slow*/continuous phenomena (such as orbit perturbations) and $\dot{n}^{+} - \dot{n}^{-}$ represents the sources and sinks of the system, so it can model *fast*/discontinuous events.

In this Section, neither sources nor sinks are considered. Hence, the continuity equation can be expressed as

$$\frac{\partial n}{\partial t} + \nabla \cdot (n\mathbf{f}) = 0 \tag{8}$$

where the term $\nabla \cdot (n\mathbf{f})$ models, in this case, the atmospheric drag effect.[10] In this approach, the radial distance r is the only spatial coordinate, so spherical symmetry is assumed. For that reason and since the atmospheric drag is the only considered perturbation, this formulation is only applicable after the band formation.

The vector field has then only one component:

$$f_r = v_r \tag{9}$$

where v_r is the drift velocity in the radial direction due to drag. According to the derivations in Letizia et al.,[8] under the hypothesis of quasi-circular orbits, v_r can be written as

$$v_r = -\varepsilon\sqrt{r}\exp\left(-\frac{r-R_h}{H}\right) \tag{10}$$

with $R_h = R_E + h_{ref}$ and the parameter ε collecting all the terms that do not depend on r:

$$\varepsilon = \sqrt{\mu_E} c_d \frac{A}{M}\rho_{ref} \tag{11}$$

where μ_E is the Earth's gravitational constant; c_d is the drag coefficient of the fragment, assumed to be constant and equal to 2.2;[17] A is the fragment cross-sectional area; and M is the fragment mass.

Using the method of the characteristics, the continuity equation (Equation 8) can be written as a system of ordinary differential equations describing the evolution in time of the density function along the characteristic lines:

$$\begin{aligned} \frac{dr}{dt} &= v_r = -\varepsilon\sqrt{r}\exp\left(-\frac{r-R_h}{H}\right) \\ \frac{dn}{dt} &= -\left[\frac{2}{r}v_r + v_r'\right] n(r,t) \end{aligned} \tag{12}$$

with initial conditions

$$\begin{aligned} r(t_0 = T_B) &= r_0 \\ n(r_0, t_0 = T_B) &= n_0(r_0) \end{aligned} \tag{13}$$

Results

In this Section, three different scenarios are considered:

- **Scenario 1:** Rocket-body explosion, in an 800-km altitude equatorial, circular orbit. The NASA breakup model is implemented considering a value of the unitless factor $S = 1$ (see Equation 1).
- **Scenario 2:** Non-catastrophic collision between a spacecraft and a 1-kg projectile with a relative impact velocity of 1 km/s. The orbit of the considered spacecraft is equatorial and circular, with an altitude equal to 800 km.
- **Scenario 3:** Catastrophic collision reproducing the Cosmos 2251 - Iridium 33 encounter in 2009.[21] The collision's initial conditions are extracted from Tan et al.[22] The orbit of the Iridium 33[22] is selected as parent orbit.

The results below correspond to a particular run of the NASA breakup model.

In Table 1, the values of the main parameters characterizing the produced fragmentation clouds are reported.

	Number of generated fragments	Number of fragments at the band formation	Band formation time
Scenario 1	378333	372442	3068.5 days
Scenario 2	13487	12867	314.94 days
Scenario 3	3182831	3012651	1660.0 days

Table 1: Parameters characterizing the generated fragmentation clouds.

In Figure 2, an alternative representation of the Gabbard diagram[23] is presented, for two different time instants: right after the fragmentation event and at the band formation. As illustrated in Figures 2a, 2c and 2e, immediately after the breakup, the fragments' distribution forms a v-shaped curve centered at the altitude where the fragmentation event occurs. The leg on the left represents the fragments whose orbit's apogee is at the breakup location, while the leg on the right shows those with the perigee at the breakup location. Figures 2b, 2d and 2f, instead, refer to the fragments' distribution at the band formation. As can be noticed, the number of fragments is reduced, since some of them have re-entered through the atmosphere. Moreover, due to atmospheric drag, the apogee altitudes decrease over time; this effect is more perceptible for fragments with low semi-major axis, which are now on circular orbits. Consequently, at the band formation, the leg on the left of the v-shaped distribution disappears.

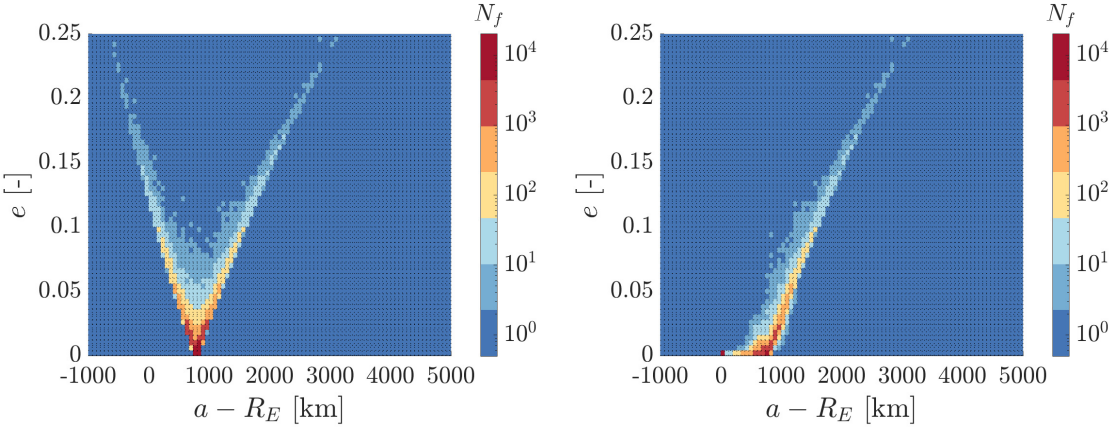

(a) Scenario 1 ($\mathbf{t_0}$)

(b) Scenario 1 ($\mathbf{t_0}$ **+ 3068 days**)

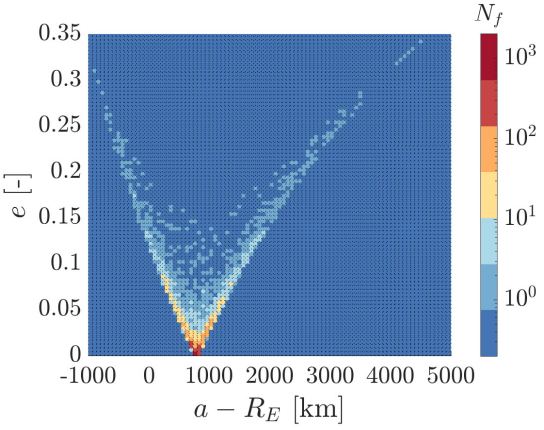

(c) Scenario 2 ($\mathbf{t_0}$)

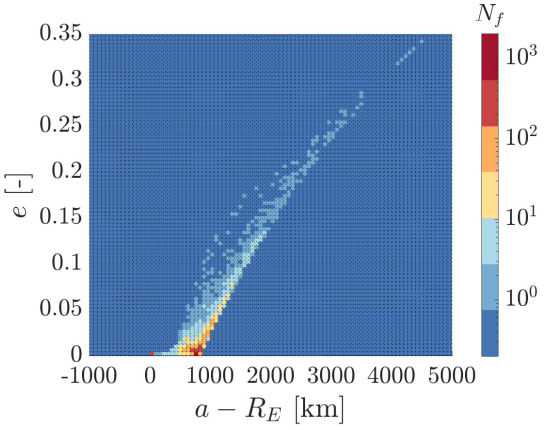

(d) Scenario 2 ($\mathbf{t_0}$ **+ 315 days**)

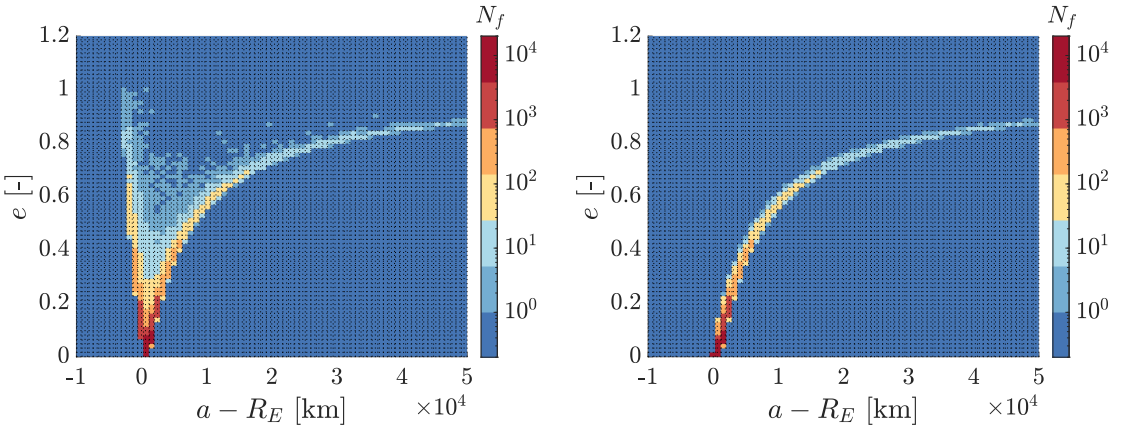

(e) Scenario 3 ($\mathbf{t_0}$)

(f) Scenario 3 ($\mathbf{t_0}$ **+ 1660 days**)

Figure 2: Distribution of semi-major axis and eccentricity, immediately after the fragmentation event (left) and at the band formation (right).

As an additional remark, in Scenario 3, some fragments with eccentricity values higher than one are generated. The fact that the proposed formulation cannot deal with these fragments does not represent a limitation. Following their parabolic and hyperbolic orbits, the fragments will escape before the band is formed and, hence, they will have no contribution to the spatial density function. Therefore, they are discarded from the set of produced fragments.

The time evolution of the spatial density function is presented in Figure 3. The fragmentation cloud is divided into seven A/M bins, each one containing the same number of objects at the band formation. The continuity equation is then integrated for each bin separately, taking the average area-to-mass ratio in the bin. As can be observed, for low values of A/M, there is a noticeable peak in the density profile even after 1000 days. Instead, for high values of A/M, the peak is less marked and rapidly decays with time, since, in this case, the drag effect is predominant.

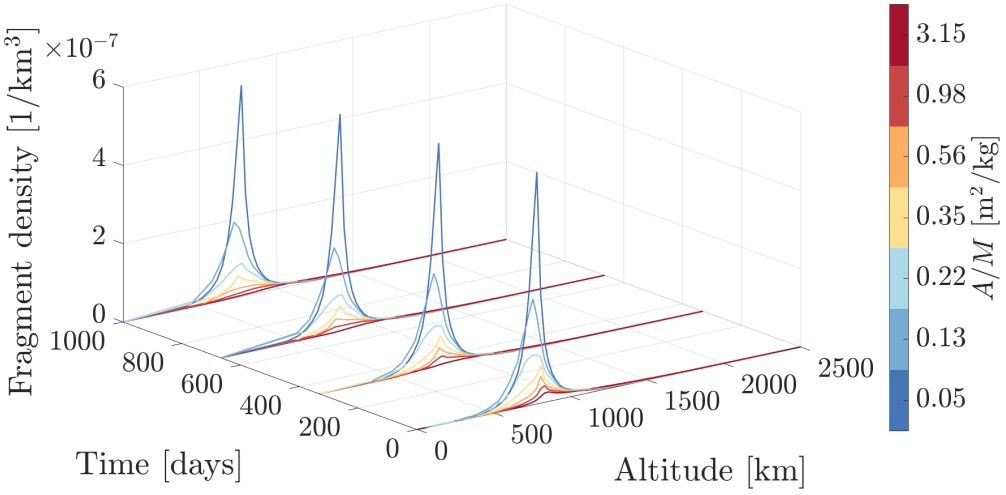

(a) Scenario 1

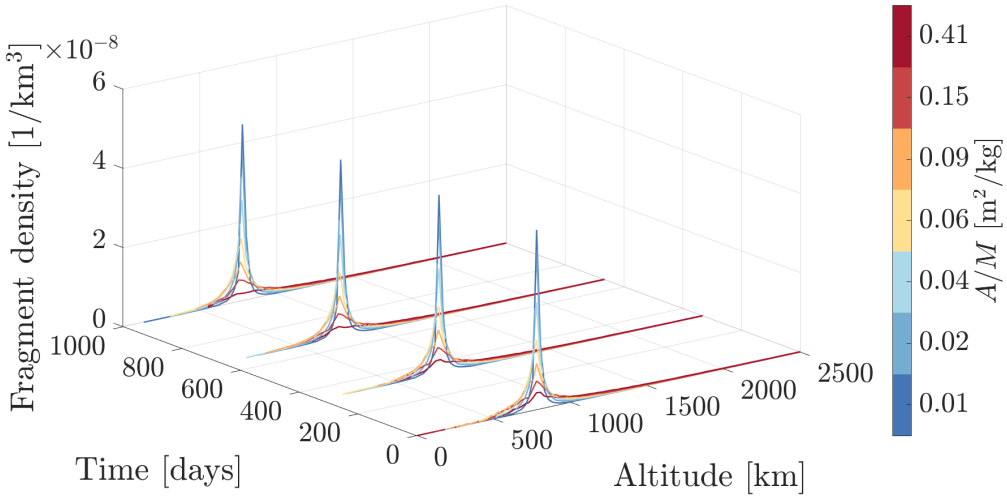

(b) Scenario 2

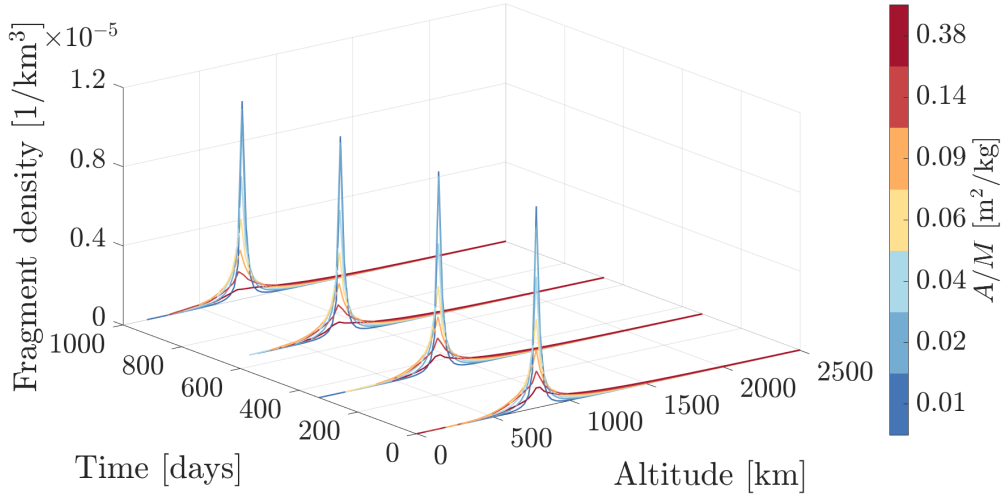

(c) Scenario 3

Figure 3: Time evolution of the fragmentation's spatial density function under drag effect (time origin set at the band formation instant).

As stated before, after the band formation, the assumption of quasi-circular orbits is imposed. To critically assess the accuracy of this hypothesis, the eccentricity distributions have been analyzed at the band formation. For all the considered scenarios, most eccentricity values were well below 0.1. Consequently, even if the proposed formulation is not well-suited for highly eccentric orbits, their contribution to the spatial density function is small and, hence, the loss of accuracy can be considered reasonable.

Finally, the dependence on the breakup altitude is analyzed. For this purpose, the dilution time is defined as the time it takes for the density peak to halve its value. As illustrated in Figure 4, both the altitude and the area-to-mass ratio have a significant effect on the dilution time, since both variables

heavily influence the intensity of the atmospheric drag force:

1. The dilution time increases for increasing breakup altitudes.

2. The dilution time increases for decreasing values of the area-to-mass ratio.

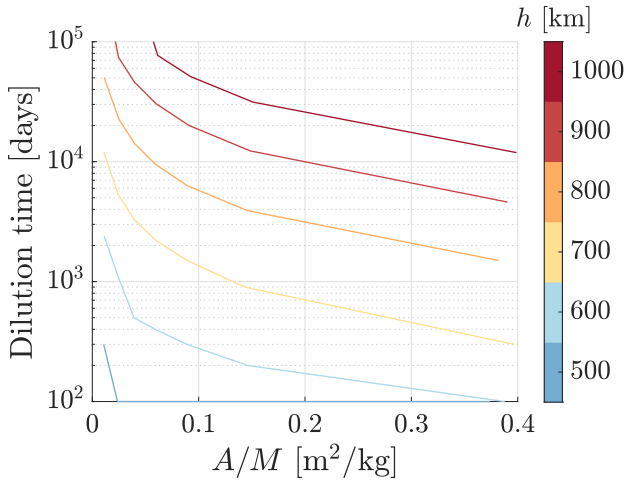

Figure 4: Dilution time as a function of area-to-mass ratio and breakup altitude (Scenario 2).

CONTINUUM FORMULATION FOR THE GLOBAL DEBRIS POPULATION

For the purpose of studying the impact of a possible collision or explosion into the overall space environment, the evolution of the entire debris population is analyzed, when at a certain instant a fragmentation event takes place. The adopted strategy is summarized in Figure 5. The IADC population is used as background debris population. Similarly to Colombo et al.,[9] the impact of the fragmentation is modelled by superimposition of effects.

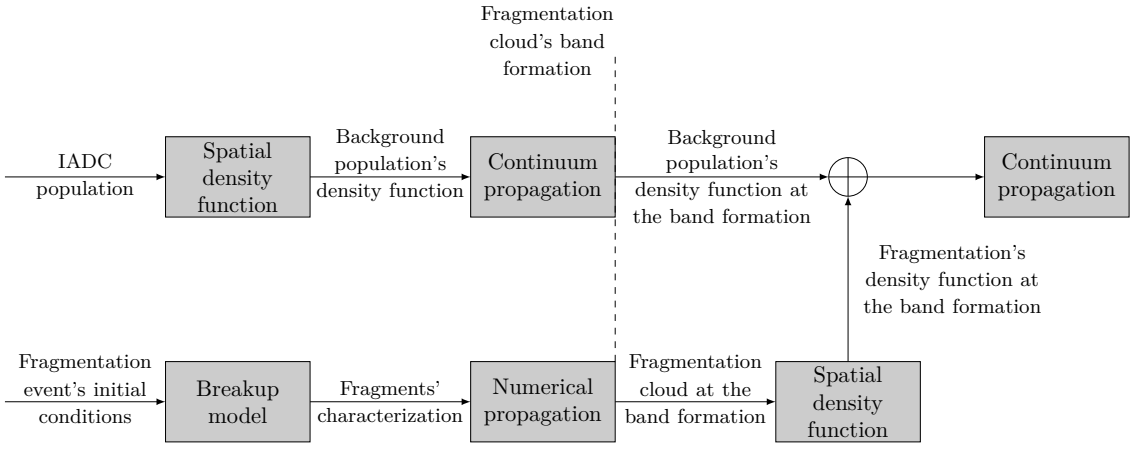

Figure 5: Schematics of the algorithm for the propagation of the total debris population, under atmospheric drag effect.

At the initial time, the spatial density function of the background population is computed and it is propagated in time according to the continuum formulation previously described. Simultaneously, the NASA breakup model is used to characterize the fragments generated from the collision or explosion, in terms of number, size, area-to-mass ratio and velocity. The orbital elements of the produced fragments are propagated up to the band formation, when the continuum approach becomes applicable also for the fragmentation cloud. At this time instant, the spatial density function of the fragmentation is built and its contribution is added to the pre-existing debris population. Finally, the resulting spatial density function is propagated again, obtaining the evolution in time of the total debris population under atmospheric drag effect.

Results

In Figure 6, the spatial density function corresponding to the background debris population at the band formation instant is presented, before and after adding the fragmentation's contribution. Again, the background population is divided into seven area-to-mass ratio bins, each one containing the same number of objects at the initial time. At the band formation, the same A/M binning is considered: the contribution of each new fragment is added to the corresponding bin, according to its area-to-mass ratio. Hence, after the band is formed, each curve accounts for the contribution of a different number of objects.

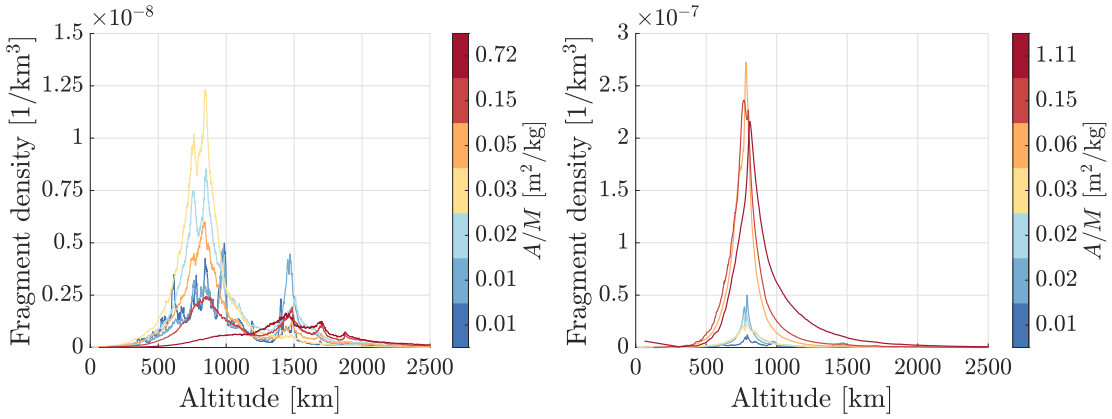

(a) Scenario 1, without fragmentation's contribution

(b) Scenario 1, with fragmentation's contribution

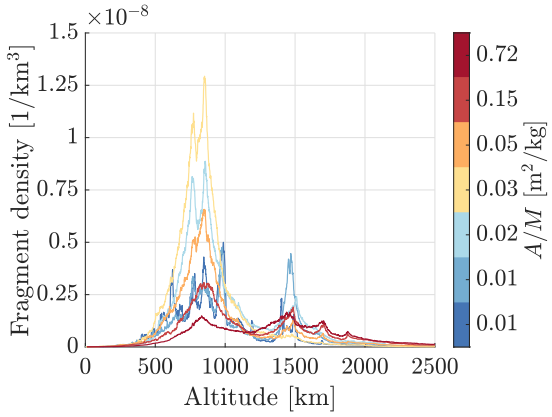

(c) Scenario 2, without fragmentation's contribution

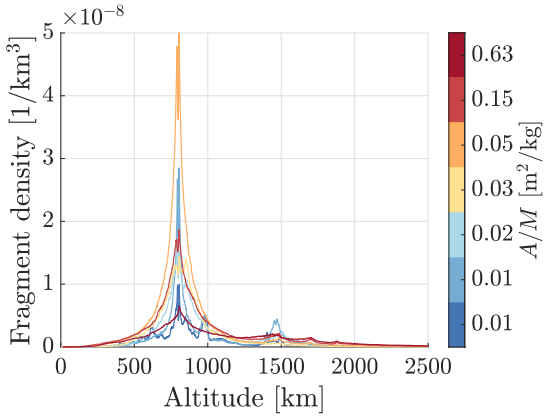

(d) Scenario 2, with fragmentation's contribution

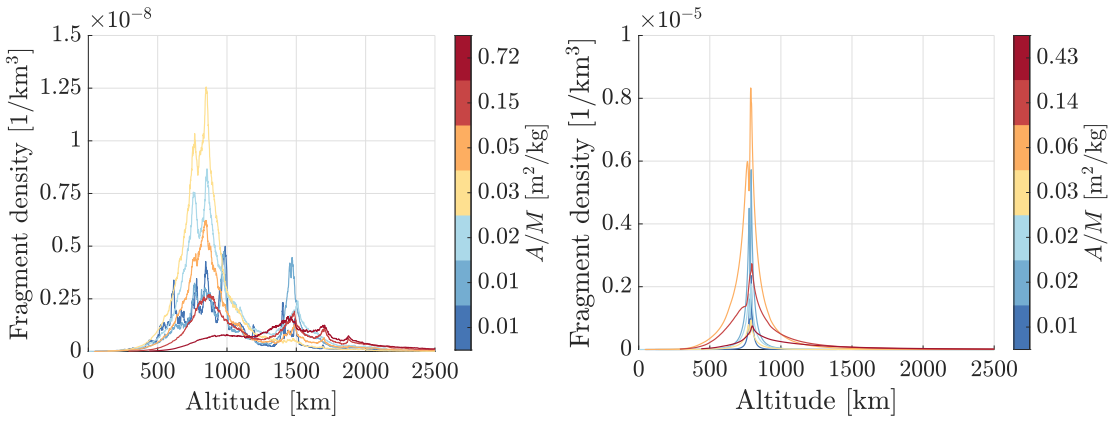

(e) Scenario 3, without fragmentation's contribution (f) Scenario 3, with fragmentation's contribution

Figure 6: Spatial density function at the band formation, before (left) and after (right) adding the fragmentation's contribution.

As can be noticed, the considered fragmentation events have dramatic effects on the total debris population. In Scenarios 1 and 2, the increase of the spatial density function is higher than 1000% at the altitude where the breakup occurs, whereas, for Scenario 3, the spatial density function undergoes a thousandfold growth at the collision altitude.

The evolution in time of the total spatial density function is shown in Figure 7, from the band formation instant. As illustrated, in addition to the dramatic increase of the spatial density function, the fragmentation events have further consequences. Drag effect is minimal for fragments with low area-to-mass ratio; consequently, these new generated fragments will remain in orbit for long periods of time, exacerbating the space debris issue.

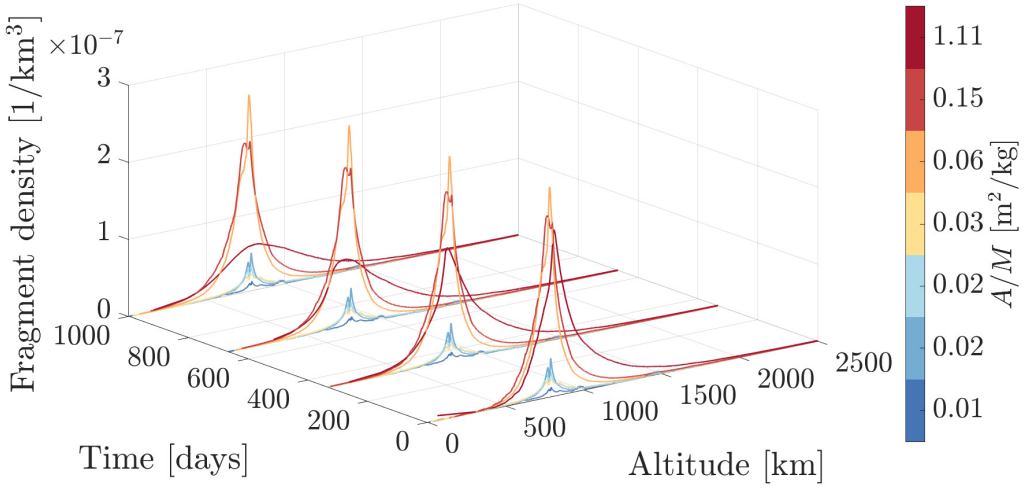

(a) Scenario 1

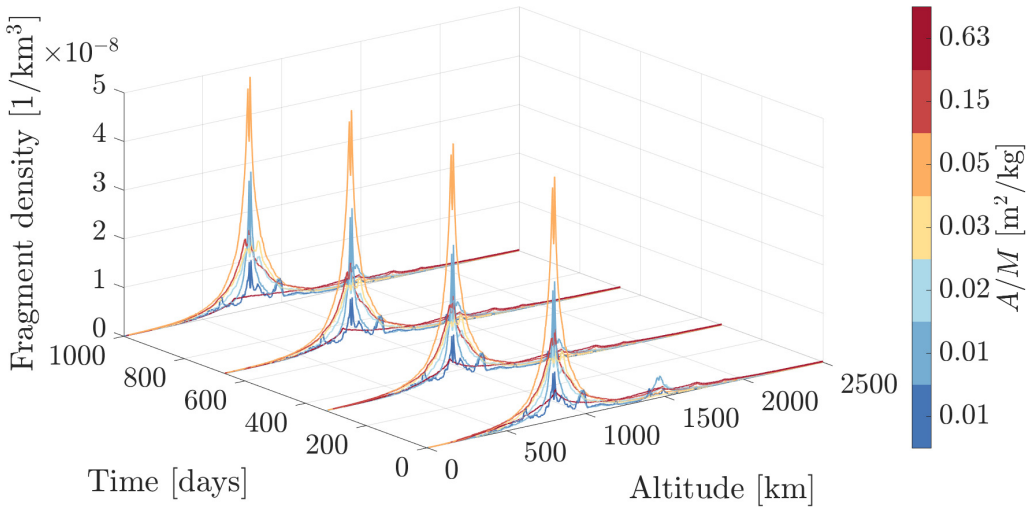

(b) Scenario 2

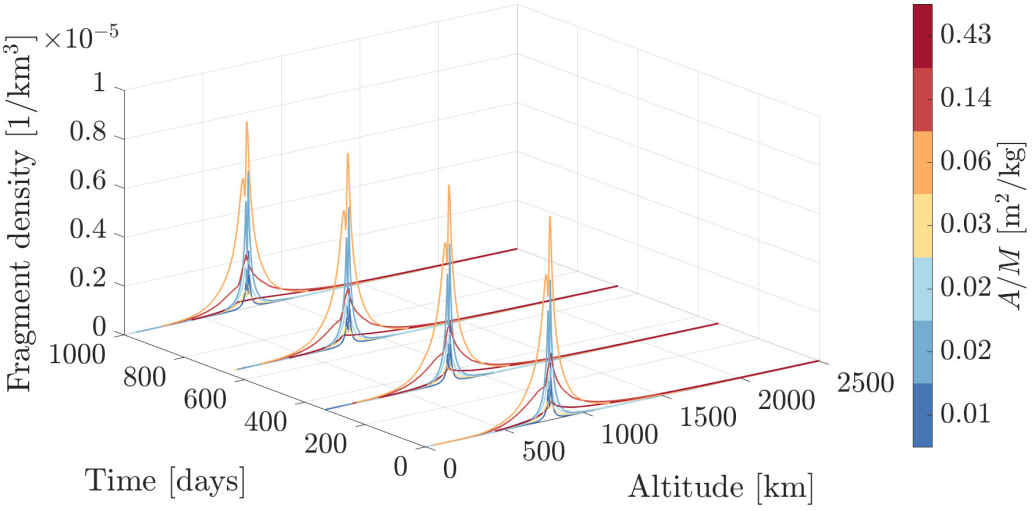

(c) Scenario 3

Figure 7: Time evolution of the total spatial density function under drag effect (time origin set at the band formation instant).

FEEDBACK EFFECT: CHAIN COLLISIONS

As a novelty, in this paper, the impact of a fragmentation event is studied by also taking into account the effect of the secondary phenomena derived from a collision or explosion in space.

The starting idea is that a fragmentation event may have not a single but a double effect on the debris population. The primary effect is a sudden increase on the number and density of space debris. However, this increase might, in turn, trigger a series of concatenated collisions, which would have a feedback effect on the global population, modifying the predicted evolution of the spatial density function.

The approach in Somma et al.[11] (which accounts for the effect of collisions into the debris population evolution) is here adapted to the modelling of the feedback effect. This additional phenomenon is included in the continuity equation as a source-sink term, which allows to study the evolution of the total population in LEO under the combined influence of atmospheric drag and feedback effect.

The adopted strategy is summarized in Figure 8. At the initial time, the background population is represented through its spatial density function and its time evolution is computed according to the continuum formulation previously presented. Simultaneously, the breakup model is employed to characterize the fragments generated as a result of the collision or explosion. The orbital elements of the produced fragments are propagated up to the band formation, when the continuum formulation becomes applicable also for the fragmentation cloud. At this time instant, the spatial density function of the fragmentation is built and its contribution is added to the background population. Finally, the resulting spatial density function is propagated again, considering now the additional feedback effect, obtaining the evolution in time of the total debris population in LEO.

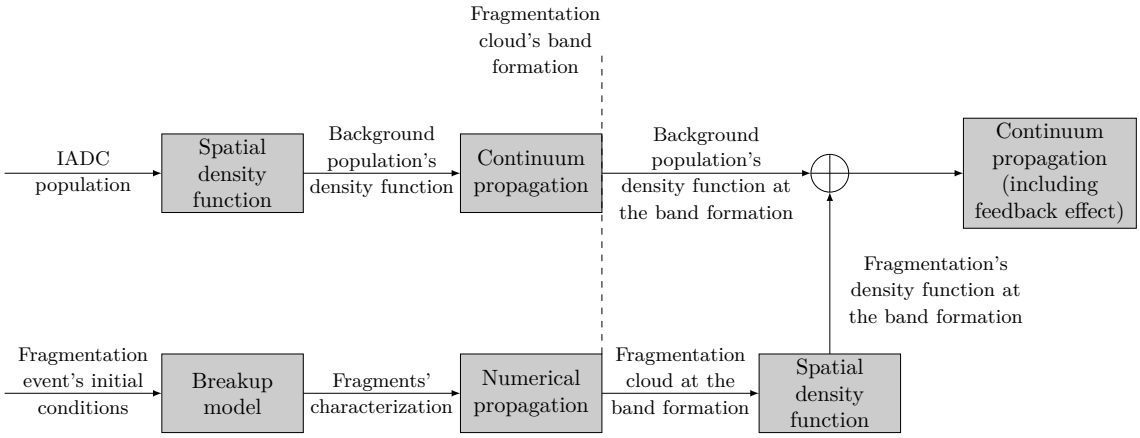

Figure 8: Schematics of the algorithm for the propagation of the total debris population, under the combined influence of atmospheric drag and feedback effect.

Formulation

Following the approach presented in Somma et al.,[11] a multi-shell and multi-species source-sink model is here adopted.

A set of first order differential equations is considered in order to determine the feedback effect's contribution to the evolution of the spatial density function. The overall debris population is divided into four different objects species: rocket bodies, payloads, mission-related objects and fragmentation debris (including both collision and explosion fragments). Again, the IADC population is considered as background debris population.

The expression in Somma et al.[11] for the population variation due to collisions is here translated into variation of the spatial density function, by merely dividing by the volume of the spherical shell of radius r and width w, $V(r, w)$:

$$\frac{dn_i(r,t)}{dt} = \sum_{j,k=1}^{N_s} \frac{C_{R_{j,k}}(r,t)}{V(r,w)} \eta_{jk,i} \quad \forall i = 1, ..., N_s \tag{14}$$

with

$$V(r,w) = 4\pi w \left(\frac{w^2}{12} + r^2 \right) \tag{15}$$

where n_i is the spatial density function of species i, N_s is the number of considered species (in this case, $N_s = 4$), $C_{R_{j,k}}$ is the collision rate among two species j and k and $\eta_{jk,i}$ is the number of objects of species i generated ($\eta_{jk,i}$ positive) or removed ($\eta_{jk,i}$ negative) as a result of a collision between objects of species j and k.

As an example, an impact between rocket bodies would remove two of them, whereas a collision between a rocket body and a payload would remove one of each kind. The number of fragments generated as a result of all the possible considered collisions is computed a priori through the NASA breakup model,[2] assuming that all the impacts between intact objects (rocket bodies, payloads and mission-related objects) are catastrophic, while all the remaining collisions are considered non-catastrophic.[11]

The collision rate among two species j and k can be computed as[11]

$$C_{R_{j,k}}(r,t) = p(r)\sigma_{j,k}\frac{N_j(r,t)[N_k(r,t) - \delta_{j,k}]}{1+\delta_{j,k}} \tag{16}$$

where N_j and N_k are, respectively, the number of objects of species j and k contained in the spherical shell of volume $V(r,w)$ at instant t; $\delta_{j,k}$ is the Kronecker's delta (equal to one if both indexes are identical; zero, otherwise); $\sigma_{j,k}$ is the square of the impact parameter, defined as the squared sum of the two objects radii, R_j and R_k:

$$\sigma_{j,k} = (R_j + R_k)^2 \tag{17}$$

and $p(r)$ is the intrinsic collision probability per unit time, as originally defined in Wetherill[24] for collisions among meteoroids in the asteroid belt:

$$p(r) = \pi \frac{\bar{v}_{rel}}{V(r,w)} \tag{18}$$

with $\bar{v}_{rel}$ the average relative velocity in the shell, assumed to be constant and equal to 10 km/s.[25–27]

Substituting in Equation 14 the expression for the collision rate:

$$\frac{dn_i(r,t)}{dt} = \sum_{j,k=1}^{N_s} \pi \bar{v}_{rel}(R_j+R_k)^2 \frac{\frac{N_j(r,t)}{V(r,w)}\left[\frac{N_k(r,t)-\delta_{j,k}}{V(r,w)}\right]}{1+\delta_{j,k}} \eta_{jk,i} \quad \forall i = 1,...,N_s \tag{19}$$

In the original formulation,[11] the variables $N(r,t)$ and w are linked, since, as previously mentioned, $N(r,t)$ is the number of objects contained in the spherical shell of radius r and width w. Here, accordingly to the definition of the spatial density function, an infinitesimal shell width is considered; thus, the discrete formulation in Somma et al.[11] is converted into a continuous approach:

$$\frac{dn_i(r,t)}{dt} = \lim_{w\to 0} \sum_{j,k=1}^{N_s} \pi \bar{v}_{rel}(R_j+R_k)^2 \frac{\frac{N_j(r,t)}{V(r,w)}\left[\frac{N_k(r,t)-\delta_{j,k}}{V(r,w)}\right]}{1+\delta_{j,k}} \eta_{jk,i} \quad \forall i = 1,...,N_s \tag{20}$$

Note that the term $\left[\frac{N_k(r,t)-\delta_{j,k}}{V(r,w)}\right]$ in Equation 20 cannot be negative, since it would imply that intact objects can be regenerated by colliding between them; here, under these conditions (e.g. in the case $j = k$), the term is imposed to be zero. Consequently, collisions among the same species are not considered, as a direct consequence of the transformation of the selected discrete formulation into a continuous one. Note that the denominator in Equation 20 is always equal to one, since the case $j = k$ is no longer considered.

Hence, the expression accounting for the feedback effect on the spatial density function evolution can be written as

$$\frac{dn_i(r,t)}{dt} = \sum_{\substack{j,k=1 \\ j\neq k}}^{N_s} \pi \bar{v}_{rel}(R_j + R_k)^2 n_j(r,t) n_k(r,t) \eta_{jk,i} \quad \forall i = 1, ..., N_s \tag{21}$$

The contribution of the feedback effect is included in the continuity equation as a source-sink term, since its dynamics is much faster than orbit perturbations dynamics. The expression of the continuity equation is here particularized, with the term $\nabla \cdot (n\mathbf{f})$ modelling the atmospheric drag and $\dot{n}^+ - \dot{n}^-$ accounting for the feedback effect:

$$\begin{aligned} &\frac{\partial n_i(r,t)}{\partial t} + v_r \frac{\partial n_i(r,t)}{\partial r} + \left(\frac{2}{r} v_r + v_r'\right) n_i(r,t) \\ &= \sum_{\substack{j,k=1 \\ j\neq k}}^{N_s} \pi \bar{v}_{rel}(R_j + R_k)^2 n_j(r,t) n_k(r,t) \eta_{jk,i} \quad \forall i = 1, ..., N_s \end{aligned} \tag{22}$$

The method of characteristics allows to obtain the set of differential equations describing the time evolution of the spatial density function along the characteristic lines, under the combined influence of atmospheric drag and feedback effect:

$$\begin{aligned} \frac{dr}{dt} &= v_r = -\varepsilon \sqrt{r} \exp\left(-\frac{r - R_h}{H}\right) \\ \frac{dn_i}{dt} &= -\left(\frac{2}{r} v_r + v_r'\right) n_i(r,t) \\ &\quad + \sum_{\substack{j,k=1 \\ j\neq k}}^{N_s} \pi \bar{v}_{rel}(R_j + R_k)^2 n_j(r,t) n_k(r,t) \eta_{jk,i} \quad \forall i = 1, ..., N_s \end{aligned} \tag{23}$$

with initial conditions

$$\begin{aligned} r(t_0 = T_B) &= r_0 \\ n_i(r_0, t_0 = T_B) &= n_{i_0}(r_0) \end{aligned} \tag{24}$$

Results

For the sake of conciseness, results are presented only for Scenario 1. Similar results are obtained for the remaining scenarios.

In Figure 9, the spatial density function of the background population is represented, at the band formation, before and after adding the fragmentation's contribution. As can be observed, now, the population is divided into species, instead of considering an A/M binning. Consequently, in this case, the differential equations corresponding to all the species are integrated together, considering an averaged area-to-mass ratio for the full debris population.

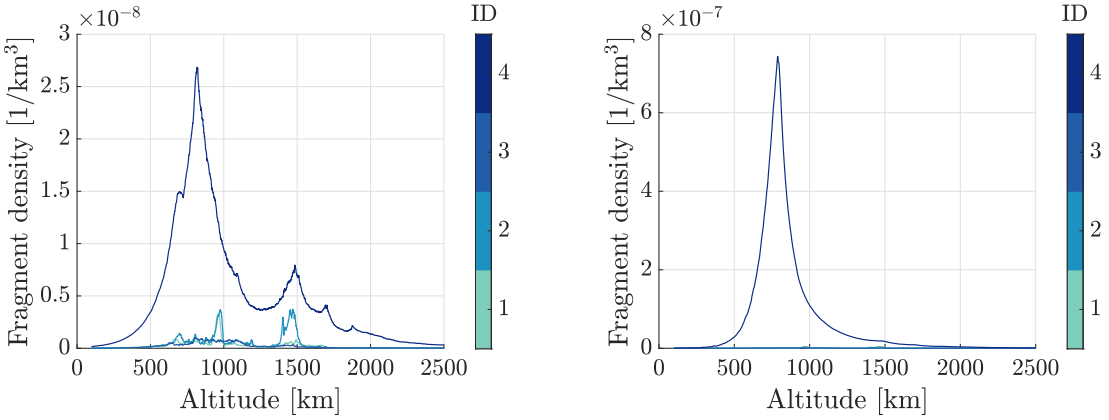

(a) Without fragmentation's contribution

(b) With fragmentation's contribution

Figure 9: Spatial density function at the band formation, before and after adding the fragmentation's contribution (Scenario 1). Species '1', '2', '3' and '4' refer, respectively, to rocket bodies, payloads, mission-related objects and fragmentation debris.

The time evolution of the density peak is presented in Figure 10; the peak height is normalized with the value at the band formation.

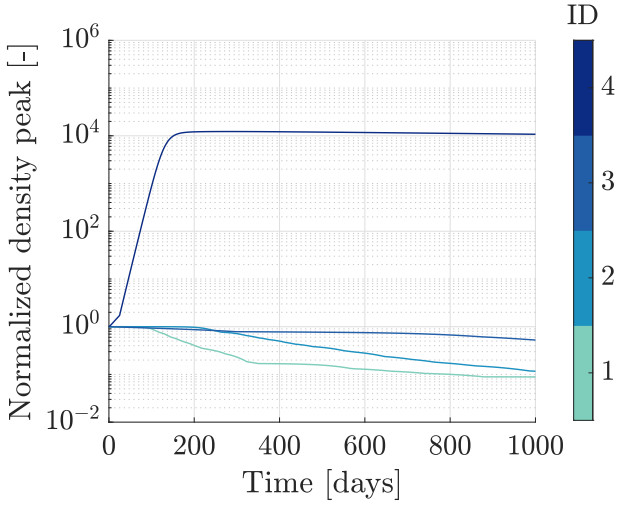

Figure 10: Evolution of the normalized density peak, under the combined influence of drag and feedback effect, for Scenario 1 (time origin set at the band formation instant). Species '1', '2', '3' and '4' refer, respectively, to rocket bodies, payloads, mission-related objects and fragmentation debris.

As illustrated, in absence of sources of intact objects (launches), three phases can be clearly dis-

tinguished. In the first phase, immediately after the band formation, all the spatial density functions are relatively small and, consequently, the evolution of the density peak height is governed by atmospheric drag. Instead, the feedback effect controls the second phase, when the fragmentation debris peak increases quadratically (while the density peaks of the intact objects decrease) up to a tipping point. From this point on (third phase), the spatial density functions of the intact objects are so small that no significant amount of new fragmentation debris is generated (since collisions among the same species are not considered) and, hence, the atmospheric drag effect overcomes the feedback effect.

In Figure 11, the evolution of the normalized density peak is shown, for each considered species.

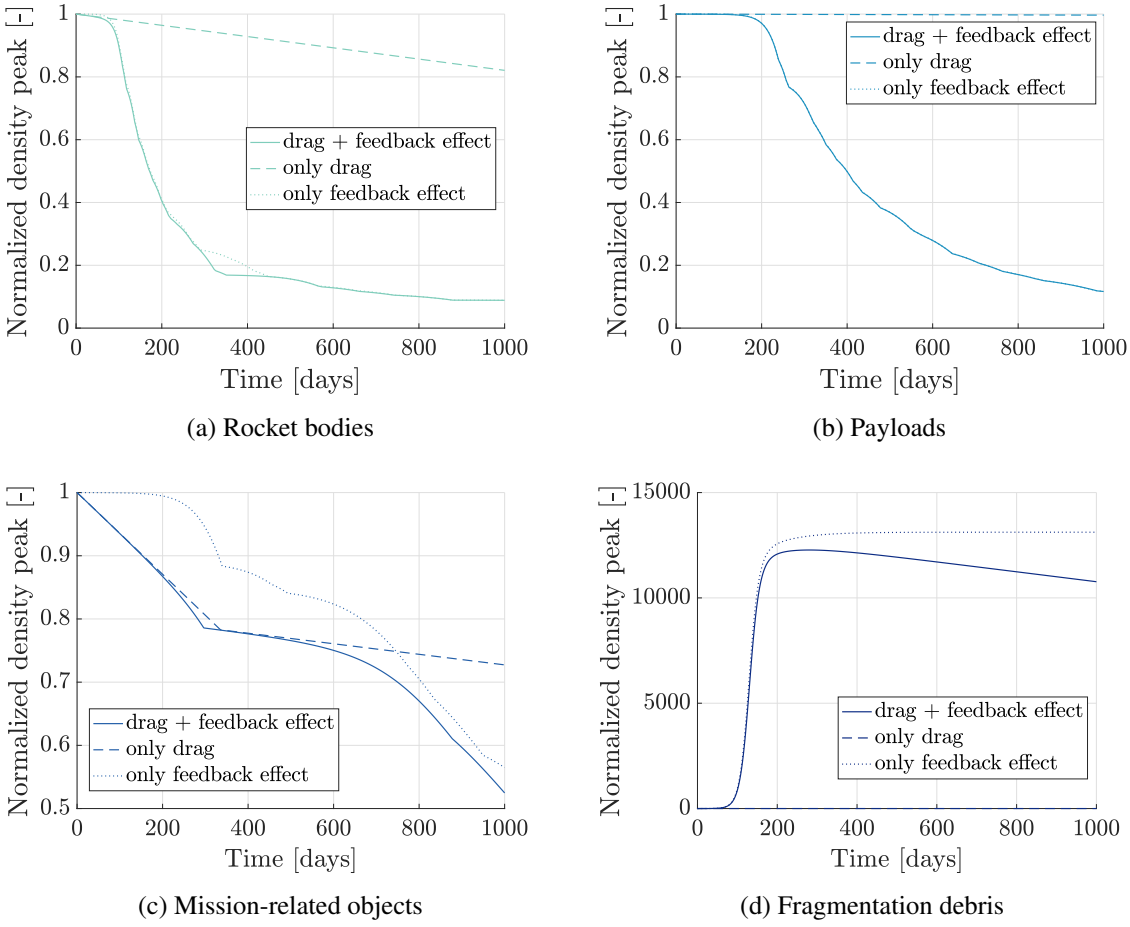

(a) Rocket bodies

(b) Payloads

(c) Mission-related objects

(d) Fragmentation debris

Figure 11: Evolution of the normalized density peak, under the individual and combined influence of drag and feedback effect, for Scenario 1 (time origin set at the band formation instant).

As can be noticed, for intact objects (rocket bodies, payloads and mission-related objects) the density peak always decreases, both under the independent influence of drag and feedback effect, even though the decrease is higher for this latter case. Instead, for the fragmentation debris, if the atmospheric drag effect were not present, the density peak would always increase until reaching a state of saturation. However, under the combined influence of atmospheric drag and feedback effect, such state of saturation is never achieved since, when the production of new fragments is no longer

significant, the atmospheric drag effect becomes dominant, leading to a density peak decrease after the tipping point.

CONCLUSION

The modelling of small debris fragments requires methods that do not rely on the propagation of single objects; within this context, density-based models offer an interesting alternative. A method based on the continuity equation is here proposed in order to analyze the impact of a fragmentation event into the global debris population, in terms of spatial density variations. Additionally, the impact of a possible chain of concatenated collisions, triggered by a single original fragmentation event, is studied, as well as its feedback effect on the overall debris population in LEO. This feedback effect is modelled through a continuum formulation and included in the continuity equation as a source-sink term, which allows to analyze the evolution of the total debris population in LEO under the combined influence of atmospheric drag and feedback effect.

In the light of the obtained results, the effect of a collision or explosion is disastrous for the global space environment, causing a dramatic increase in the debris spatial density function. In addition, the long-term repercussions of fragmentation events are revealed. Since the drag effect is minimal for fragments with low area-to-mass ratio, a great portion of these new generated fragments will stay in orbit for a long time. The feedback effect further aggravated the debris situation, severely increasing the fragmentation debris population after a collision or explosion takes place.

ACKNOWLEDGEMENTS

This work has received funding from the Italian Space Agency, in the framework of the ASI-INAF Agreement "Supporto alle attività lADC e validazione pre-operativa per SST (N. 2020-6-HH.0)."

REFERENCES

[1] Space Debris Program Office, "Monthly Effective Mass of Objects in Earth Orbit by Region," *Orbital Debris Quarterly News*, Vol. 19, No. 1, 2015, p. 9.

[2] N. Johnson and P. Krisko, "NASA's New Breakup Model of Evolve 4.0," *Advances in Space Research*, Vol. 28, No. 9, 2001, pp. 1377–1384.

[3] A. Rossi, A. Cordelli, C. Pardini, L. Anselmo, and P. Farinella, "Modelling the Space Debris Evolution: Two New Computer Codes," *Advances in the Astronautical Sciences*, Vol. 89, 1995, pp. 1217–1231.

[4] H. G. Lewis, A. E. White, R. Crowther, and H. Stokes, "Synergy of Debris Mitigation and Removal," *Acta Astronautica*, Vol. 81, No. 1, 2012, pp. 62–68.

[5] J.-C. Liou, D. Hall, P. Krisko, and J. Opiela, "LEGEND – A Three-Dimensional LEO-to-GEO Debris Evolutionary Model," *Advances in Space Research*, Vol. 34, No. 5, 2004, pp. 981–986.

[6] P. H. Krisko, "The Predicted Growth of the Low-Earth Orbit Space Debris Environment — an Assessment of Future Risk for Spacecraft," *Proceedings of the Institution of Mechanical Engineers, Part G: Journal of Aerospace Engineering*, Vol. 221, No. 6, 2007, pp. 975–985.

[7] L. Anselmo, A. Rossi, and C. Pardini, "Updated Results on the Long-Term Evolution of the Space Debris Environment," *Advances in Space Research*, Vol. 23, No. 1, 1999, pp. 201–211.

[8] F. Letizia, C. Colombo, and H. G. Lewis, "Analytical Model for the Propagation of Small-Debris-Object Clouds After Fragmentations," *Journal of Guidance, Control, and Dynamics*, Vol. 38, No. 8, 2015, pp. 1478–1491.

[9] C. Colombo, F. Letizia, and H. Lewis, "Spatial Density Approach for Modelling of the Space Debris Population," *26th AAS/AIAA Space Flight Mechanics Meeting*, February 2016, pp. 2749–2761.

[10] C. R. McInnes, "Simple Analytic Model of the Long-Term Evolution of Nanosatellite Constellations," *Journal of Guidance, Control, and Dynamics*, Vol. 23, No. 2, 2000, pp. 332–338.

[11] G. L. Somma, C. Colombo, and H. Lewis, "A Statistical LEO Model to Investigate Adaptable Debris Control Strategies," *7th European Conference on Space Debris, ESA/ESOC*, April 2017.

[12] P. H. Krisko, "Proper Implementation of the 1998 NASA Breakup Model," *Orbital Debris Quarterly News*, Vol. 15, No. 4, 2011, pp. 1–10.

[13] F. Letizia, *Space Debris Cloud Evolution in Low Earth Orbit*. PhD thesis, University of Southampton, November 2015.

[14] L. Olivieri, C. Giacomuzzo, C. Duran-Jimenez, A. Francesconi, and C. Colombo, "Fragments Distribution Prediction for ENVISAT Catastrophic Fragmentation," *8th European Conference on Space Debris, ESA/ESOC*, ESA, 2021, pp. 1–12.

[15] R. Jehn, "Dispersion of Debris Cloud from In-Orbit Fragmentation Events," *ESA Journal*, Vol. 15, No. 1, 1991, pp. 63–77.

[16] J. Ashenberg, "Formulas for the Phase Characteristics in the Problem of Low-Earth-Orbital Debris," *Journal of Spacecraft and Rockets*, Vol. 31, No. 6, 1994, pp. 1044–1049.

[17] D. A. Vallado, *Fundamentals of Astrodynamics and Applications, 4th Edition*. New York, NY: Springer, 2013.

[18] D. King-Hele, *Satellite Orbits in an Atmosphere: Theory and Application*. Glasgow and London: Blackie, 1987.

[19] D. J. Kessler, "Derivation of the Collision Probability between Orbiting Objects: the Lifetimes of Jupiter's Outer Moons," *Icarus*, Vol. 48, No. 1, 1981, pp. 39–48.

[20] S. Frey, C. Colombo, S. Lemmens, *et al.*, "Application of Density-Based Propagation to Fragment Clouds using the Starling Suite," *1st International Orbital Debris Conference (IOC)*, 2019, pp. 1–10.

[21] C. Pardini and L. Anselmo, "Review of Past On-Orbit Collisions among Cataloged Objects and Examination of the Catastrophic Fragmentation Concept," *Acta Astronautica*, Vol. 100, 2014, pp. 30–39.

[22] A. Tan, T. Zhang, and M. Dokhanian, "Analysis of the Iridium 33 and Cosmos 2251 Collision using Velocity Perturbations of the Fragments," *Advances in Aerospace Science and Applications*, Vol. 3, No. 1, 2013, pp. 13–25.

[23] D. S. F. Portree and J. P. Loftus, "Orbital Debris: A Chronology," 1999.

[24] G. W. Wetherill, "Collisions in the Asteroid Belt," *Journal of Geophysical Research*, Vol. 72, No. 9, 1967, pp. 2429–2444.

[25] D. L. Talent, "Analytic Model for Orbital Debris Environmental Management," *Journal of Spacecraft and Rockets*, Vol. 29, No. 4, 1992, pp. 508–513.

[26] C. Pardini and L. Anselmo, "Review of Past On-Orbit Collisions among Cataloged Objects and Examination of the Catastrophic Fragmentation Concept," *Acta Astronautica*, Vol. 100, 2014, pp. 30–39.

[27] D. J. Kessler, "Orbital Debris Environment for Spacecraft in Low Earth Orbit," *Journal of Spacecraft and Rockets*, Vol. 28, No. 3, 1991, pp. 347–351.